J Nanostruct Chem (2016) 6:261–274
DOI 10.1007/s40097-016-0199-9

ORIGINAL RESEARCH

Photocatalytic oxidation of phenol red onto nanocrystalline TiO_2 particles

Hilal S. Wahab[1] · **Ahmed A. Hussain**[1]

Received: 15 April 2016 / Accepted: 11 June 2016 / Published online: 23 June 2016

Abstract The employment of UV/TiO_2/O_2/H_2O_2 system for the degradation of phenol red in aqueous solutions using synthesized nanosized TiO_2 powder has been investigated in the present study. The anatase TiO_2 nanoparticles were synthesized using sol-gel methodology and characterized spectroscopically exploiting SEM, TEM, XRD, and DUR–UV–VIS, in addition to BET analysis. We observe that the degradation of the dye depends on several operational parameters, such as initial pH, catalyst dosage, initial concentration of the dye, UV light intensity, irradiation time, catalyst particle size, and the presence of electron acceptors, such as hydrogen peroxide, besides molecular oxygen. Kinetic analyses indicate that the photodegradation rates of phenol red dye follow the pseudo-first-order kinetics according to the Langmuir–Hinshelwood model. The influence of temperature in the range 25–45 °C was studied. The degradation kinetics were somewhat accelerated by increase in temperature, and apparent activation energy was calculated to be 38.23 kJ mol^{-1}. Thermodynamic parameters, $\Delta H^{\#}$, $\Delta G^{\#}$, and $\Delta S^{\#}$ of activation were also computed for the degradation process.

Keywords Phenol red · Anatase · TiO_2 · Photocatalysis · Langmuir · Heterogeneous

Abbreviations

SEM	Scanning electron microscopy
EDXS	Energy dispersive X-ray spectroscopy
XRD	X-ray diffraction
DUR–UV–VIS	Diffused reflectance UV–VIS spectrometry
TEM	Transmission electron microscopy
BET	Brunauer–Emmett–Teller
UV–VIS	Ultra violet-visible spectrophotometer
FTIR	Fourier transform infrared spectroscopy
k_{app}	Apparent first-order rate constant
AOP	Advanced oxidation process
COD	Chemical oxygen demand
TOC	Total organic carbon
E_g	Band gap energy
4-CP	4-Chlorophenol
pzc	Point of zero charge
K_{ad}	Adsorption equilibrium coefficient
MPML	Medium-pressure mercury lamp
TDS	Total dissolved solids
STEM	Super transmission electron microscope
BF/DF	Bright field/dark field detectors
FWHM	Full width at half maximum
L–H	Langmuir–Hinshelwood
E_a	Activation energy
$\Delta G^{\#}$	Free energy of activation
$\Delta H^{\#}$	Enthalpy of activation
$\Delta S^{\#}$	Entropy of activation
k_B	Boltzmann constant
h	Planck's constant

Electronic supplementary material The online version of this article (doi:10.1007/s40097-016-0199-9) contains supplementary material, which is available to authorized users.

✉ Hilal S. Wahab
hswahab@gmail.com; hswahab@yahoo.com

[1] Department of Chemistry, College of Science, Al-Nahrain University, P.O. Box 64090, Al-Jadriya, Baghdad, Iraq

Introduction

Aromatic compounds and their phenolic derivatives are of environmental concern, because they are extensively used for manufacturing of pesticides, dyes, explosives, solvents, and industrial chemicals or precursors. They are classified to be anthropogenic, bio-refractory [1], and extremely toxic for human beings and for all aquatic life [2]. As a result, their widespread use leads to appear as contaminants in water sources, such as surface water and industrial wastewaters [3]. Despite their low concentrations in industrial effluents and wastewaters, these contaminants ultimately enter the aquatic ecosystem, and can create various environmental hazards and also raise substantial health concern due to their extremely high endocrine disrupting potency and genotoxicity [4]. The conventional processes to remove these pollutants involve physical, chemical, and biological methods. Nevertheless, the individual application of these techniques is generally limited and cannot degrade completely the recalcitrant organic matter [5]. Semiconductor heterogeneous photocatalysis which is classified as advanced oxidation process (AOP) is a popular and suitable technique for the oxidation of recalcitrant contaminants, such as dyes and phenolic compounds [6, 7]. One of the major applications of heterogeneous catalysis is photocatalytic oxidation to promote partial or total mineralization of gas-phase or liquid-phase contaminants to benign substances. Although degradation begins with a partial degradation, the term 'photocatalytic degradation' usually refers to complete photocatalytic oxidation or photomineralisation, essentially to CO_2, H_2O, NO_3^-, $PO4^{3-}$, and halide ions [8].

Of the semiconductor materials being developed for photocatalytic applications, TiO_2 is the most suitable, because of its high oxidizing ability, long-term stability, low cost, and nontoxicity [9]. There are three morphological forms of TiO_2; rutile, anatase, and the rare mineral form, brookite. Only rutile and anatase have been considered from the catalysis viewpoint. The band gap energy of anatase phase (3.2 eV) is higher than that of rutile phase (3.0 eV); nevertheless, the anatase has been considered as more active photocatalytically than rutile [10]. This is ascribed mainly to the higher reduction potential of the photoproduced anatase electrons, of e^-/h^+ pair, which are located above hydrogen zero potential point (−0.2 eV) within the reduction zone. Garcia et al. [11] have reported in their comparative study that among processes, such as UV/H_2O_2, $UV/TiO_2/H_2O_2$, and $UV/Fe^{2+}/H_2O_2$; the association of TiO_2 and H_2O_2 was the most efficient treatment for removing organic compounds from textile effluents.

The knowledge of the main thermodynamic and kinetic factors influencing the photoreactivity is essential to make predictions on the feasibility of photoprocesses [12]. To the best of our knowledge, little is known on the photocatalytic degradation of phenol red (PR) using TiO_2 [13, 14]. Moreover, there is no data documented in the literature about the quantitative data on thermodynamic parameters relating the kinetics and photodegradation process. Therefore, in this study, phenol red was chosen as model phenolic pollutant. Phenol red possesses wide range of applications, such as bromination catalysts, pH indicator, and estrogenic properties [15–17]. Correspondingly, present study was aimed at elucidating the impacts of several processing parameters, such as initial concentration of the dye, photocatalyst dosage, initial pH, UV light intensity, initial H_2O_2 concentration, photocatalyst particle size and irradiation time on the photodegradation of this harmful material employing synthesized slurry nanoTiO_2 particles.

Experimental details

Materials

All the chemicals which have been used were as high purity as available and used without further purification. Phenol red (98 %) was purchased from Thomas Baker, titanium isopropoxide (98 %) from Acros Organics and standard nanopowder anatase TiO_2 reference specimen (particle size <25 nm, 99.7 %) from Sigma-Aldrich. Deionized water, TDS ≈ zero, was used for all experiments.

Instrumentation

For the sake of comparison, the characterization of the synthesized nanoTiO_2 photocatalyst has been conducted along with standard nanopowder anatase TiO_2 reference specimen.

The synthesized nanoTiO_2 photocatalyst characterized using the following techniques: The X-ray powder diffraction (XRD) patterns were obtained on a Philips X-pert 3040/60 XRD machine using a Cu target Kα radiation ($\lambda = 0.154056$ nm) to determine the crystalline size and to explore the phase. The accelerating voltage and the applied current were 40 kV and 30 mA, respectively. The XRD patterns were at the scanning range 2θ from 20° to 60°. UV–Vis diffuse reflectance spectra (DUR–UV–VIS) of the catalysts were recorded by a Shimadzu UV-3600 spectrophotometer coupled with a spherical integration unit to obtain the optical absorption threshold of the sample, using $BaSO_4$ as the reference sample, within the wavelength range of 200–800 nm. The Brunauer, Emmett, and Teller (BET) specific surface area and pore distribution were determined using nitrogen adsorption/desorption

isotherm, performed by Micromeritecs' Gemini surface area analyzer with nitrogen as the adsorbate, and liquid nitrogen as the sample coolant. Hitachi S-4700 FE-SEM cold field-emission high-resolution scanning electron microscope (SEM) was used to explore the morphological and structural properties of the nanopowders. Furthermore, the Hitachi HT7700 STEM (super transmission electron microscope), including bright field (BF) and dark field (DF) detectors, has been used for nanopowder orientation and particle size analysis.

Results and discussion

Characterization of the photocatalyst

The surface area, mesoporosity, particle size, morphology, and other properties of TiO_2 nanocatalyst were determined, because these characteristics are very crucial in providing the efficiency to degrade the organic compounds [18]. The nitrogen adsorption BET surface area for the prepared nanoTiO_2 powder was found to have a value of 48 m^2 g^{-1}, indicating the large surface area of the particles. Furthermore, the average pore size and pore volume were 3.7 nm and 0.067321 cm^3 g^{-1}, respectively. Hence, the large surface area and mesoporosity of the nanoparticles may enhance the speed of photocatalytic reaction, since the photocatalytic activities take place on the catalyst surface when irradiated with ultraviolet light [19, 20]. From the XRD characterization, as shown in Fig. 1S, the 2θ value for the synthesized nanoTiO_2 powder coincides with that of the reference nanoTiO_2 powder. Furthermore, there were no distinct peaks observed for rutile phase in synthesized TiO_2 nanopowder which indicates that the relatively low calcination temperature (400 °C) might be the appropriate temperature for the preparation of high-purity anatase TiO_2 nanomaterial and is also beneficial in preserving the particle size at nanoscale. The average crystalline size was calculated by Sherrer's equation using the XRD line broadening method [21]. The crystal size $D = 0.9\lambda/(B\cos\theta)$, where λ represents the wavelength of X-ray, B the FWHM, and the θ diffraction angle. Using the experimental data, an average crystalline size of 9.95 nm was derived.

The surface morphology and the approximate particle size of the mesoporous TiO_2 which were characterized by SEM are illustrated in Fig. 2S, with smooth, homogeneous surface, very similar particles shape, and average particle size of 11 nm. The surface has also been explored by high-resolution scanning transmission electron microscope (STEM) for the nanoscale analysis. The nanoparticles have an irregular spherical shape and excellent dispersivity with average size of 9 nm (Fig. 3S). On the other hand, it should be noted that the necking regions between the particles are benefit for the formation of network structure, as observed in SEM and TEM images, which is expected to be advantageous for the transport of electron in the skeleton [17].

Ground-state DUR–UV–VIS absorption spectra of solid powder for both the nanoanatase TiO_2 reference specimen and synthesized nanopowder anatase TiO_2 were measured. Figure 4S explicitly depicts the excellent accordance of absorption thresholds for both the reference and synthesized specimen at 350 nm which subsequently refer to bandgap energy (E_g) of 3.4 eV.

Factors influencing the photocatalytic degradation

Influence of pH

Some authors [22–24] reported that UV light illumination and the TiO_2 photocatalyst are the main constituents of the effective photocatalysis system of phenol red dye. However, the most important parameter in the photocatalytic reactions taking place on particulate surfaces is the pH of the solution, since it dictates the surface charge properties of the photocatalyst [8]. Cherif et al. [25] reported that the point of zero charge (pzc) of the TiO_2 was at pH 6.5 and, hence, TiO_2 surface is positively charged in acidic medium (pH <6.5) and negatively charged in alkaline medium (pH >6.5). On the other hand, Asiri et al. [13] stated that phenol red molecule exists in different molecular structures with different charge distributions (Fig. 1), depending on the pH of the solution. Whereas, Tamura and Maeda [26] stated that the phenol red in crystalline form and in solution under acidic conditions (low pH), the compound exists as a zwitterion as in the structure (b), with the sulfate group negatively charged, and the ketone group carrying an additional proton. This form is sometimes symbolically written as $H_2{}^+PS^-$ and is orange–red. If the pH is increased, the proton from the ketone group is lost, resulting in the yellow negatively charged ion denoted as HPS^- as in the structure (a). At still higher pH, the phenol's hydroxide group loses its proton, resulting in the red ion denoted as PS^{2-} as in the structure (c). Therefore, pH changes can influence the adsorption of phenol red dye molecules onto the TiO_2 surfaces. To optimize the pH of the phenol red degradation process, experiments were conducted with pH range 2–8 at a fixed catalyst dosage of 0.5 g l^{-1} and initial dye concentration of 10 ppm. We observed that phenol red degradation was favorable at mild acidic solution (pH = 4.5), as shown in Table 1. Accordingly, on the basis of this result, pH of 4.5 was taken as the optimum pH for the optimization processes. Similar results were reported by Asiri et al. [13] for the maximum photodegradation of phenol red on TiO_2 under solar irradiation

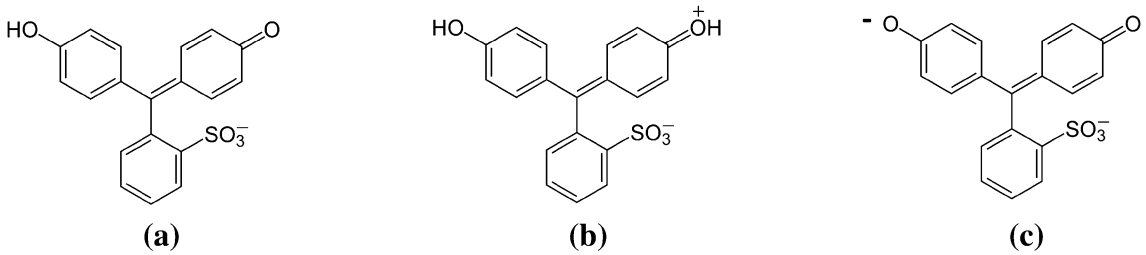

Fig. 1 Variation of phenol red molecular structure at different pH values: **a** low pH; **b** moderate pH; and **c** high pH

Table 1 Effect of pH variation on the rate of phenol red photocatalysis

PH	Rate (mol l^{-1} min) × 10^{-9}
2	23
3	24
4	28
4.5	47
5	24
6	5
8	5

Table 2 Degradation rate of phenol red at different TiO_2 loadings

TiO_2 dosage (mg)	Rate of reaction ($\times 10^{-9}$ mol l^{-1} min)
10	110
20	115
30	125
40	295
50	210
60	179
100	52

at value of pH that included in 4.4 and Oghenejoboh et al. [27] in their study of the photodegradation of chlorobenzene at pH = 3 on TiO_2.

The surface functional groups of TiO_2 in water may be $TiOH_2^+$, TiOH, and TiO^-. At $pH > pH_{zpc}$, TiO^- is the predominant species, while $TiOH_2^+$ plays the role as $pH < pH_{zpc}$ according to the following reactions [7]:

$$pH < P_{zc}TiOH + H^+ \rightarrow TiOH_2^+ \quad (1)$$

$$pH > P_{zc}TiOH + OH^- \rightarrow TiO^- + H_2O. \quad (2)$$

Wang et al. [28] have reported that the state of the chemical species presented in water is not affected only by pH, but is also closely related to the dissociation constant of the species. When pH is lower than the pK_a of the species, it primarily presents in molecular state, whereas, at pH greater than the pK_a, it exists as ionic state. The pH_{zpc} of TiO_2 used in this study is about 6.5 and the pK_a's phenol red is 8. Accordingly, under moderate acidity conditions (pH = 4.5) and based on above debate, we predict that $TiOH_2^+$ is the predominant species for TiO_2 and the structure (a) of phenol red is the primary species, which contributes appreciably in the elevation of the amount of adsorption, and, as a result, enhances the degradation rate.

Effect of TiO_2 loading

Whether in static, slurry, or dynamic flow reactors, the initial reaction rates were found to be directly proportional to catalyst concentration indicating the heterogeneous regime [29]. Hence, the loading amount of catalyst is a significant factor in the photocatalytic degradation process, because the efficiency could be strongly affected by the number of active sites and photoadsorption ability of the catalyst used, as extensively demonstrated in previous studies [30]. However, it was observed that above a certain optimum catalyst mass, the reaction rate even decreases and becomes independent of the catalyst concentration [29]. Malato et al. [31] have stated that in any given application, this optimum catalyst mass has to be found to avoid excess catalyst and ensure total absorption of efficient photons. Therefore, a TiO_2 load ranging from 10 to 100 mg was used to investigate its influence on the photocatalytic degradation rate and degradation yield of phenol red and find out the optimal loading amount. Table 2 reveals the variation in degradation rate of phenol red against the dosage of nanoanatase TiO_2. The results obtained support the behavior described by some authors [32, 33]. These studies evaluate the increase in reaction rate with catalyst loading as evidence that the process is photoactivated. The enhancement of the photodegradation rates was observed from Table 2 with the increase of TiO_2 dosage from 10 to 40 mg (0.13–0.53 g l^{-1}). This direct proportional of initial reaction rates with catalyst loading is evidently indicating the heterogeneous regime [34]. However, a further increase in loading amount had negative effect on the photocatalytic degradation of phenol red. This outcome is in a good accordance with most of studies in the literature which reported enhanced degradation rates for TiO_2 catalyst loading up to 400–500 mg l^{-1} [29, 35] This

can be attributed to the fact that increased number of TiO_2 particles will increase the availability of active sites of TiO_2 surface and number of photons absorbed. Beyond the optimal limiting value of TiO_2 loading (40 mg), the dropping in the photodegradation rate mainly results from either aggregation of TiO_2 particles at high loadings, and/or an increase in opacity and light scattering of TiO_2 particles [36]. In addition, the decreased penetration of UV light irradiation in a high TiO_2 loading attributable to light scattering and screening could result in the reduction of TiO_2 specific activity [37].

Impacts of initial dye concentration

It is important both from a mechanistic and from application perspectives to study the dependence of the photocatalytic process rate and degradation yield on the phenol red initial concentration. As a result of this, the initial dye concentration was optimized by varying the concentration of phenol red between 5 and 25 ppm at a catalyst dosage of 0.5 g l^{-1} and pH of 4.5. The effect of initial concentration on the photocatalytic degradation rate of phenol red is implied in Table 3. It is noted that the degradation rate increases with increase in phenol red concentration to a certain level, and a further increase in dye concentration leads to decrease the degradation rate of the dye. Similar phenomenon has also been reported by several researchers [25, 27]. Konstantinou and Albanis [29] stated that the rate of

degradation relates to the probability of ·OH radicals formation on the catalyst surface and to the probability of ·OH radicals reacting with dye molecules. Accordingly, as the initial concentrations of the dye increase, the probability of reaction between dye molecules and oxidizing species also increases, leading to an enhancement in the degradation rate. On the contrary, the degradation efficiency of the dye decreases, as the dye concentration increases further. The presumed reason is that at high dye concentrations, the generation of ·OH radicals on the surface of catalyst is reduced, since the active sites are covered by dye ions. This possible explanation for this behavior was verified by Andronic et al. [38] who reported that, for increasing initial dye concentrations, more organic substances are adsorbed on the surface of TiO_2, while fewer photons are available to reach the TiO_2 surface and, therefore, less hydroxyl radicals are formed, causing a decrease of the degradation efficiency. Danesshvar et al. [39] concluded in their work on azo dye acid red phocatalytic degradation that a possible cause for such phenomenon is the UV-screening effect of the dye itself. At a high dye concentration, a significant amount of UV may be absorbed by the dye molecules rather than the TiO_2 particles and that reduces the efficiency of the catalytic reaction because the concentrations of $^{\bullet}OH$ and $O_2^{\bullet-}$ decrease. Further elucidation was published by Neppolian et al. [40] who explained that the major portion of degradation occurs in the region near to the irradiated side (termed as reaction zone), where the irradiation intensity is much higher than in the other side. Hence, it is concluded that as initial concentration of the dye increases, the requirement of catalyst surface needed for the degradation also increases.

On the basis of the above debate, we can conclude that as phenol red dye concentration increases beyond the optimum (10 ppm), the degradation rate is proportional to the concentration. Similar conclusion has also made by others working on the photocatalytic degradation of 4-flurophenol, 4-CP, phenol, and *m*-nitrophenol, as well as acid blue 80 using TiO_2 and ZnO under solar irradiation [41–43].

Table 3 Variation of rate constant with phenol red initial concentration; TiO_2 dosage = 0.5 g l^{-1}, pH = 4.5; irradiation period = 5 h

Conc. (mg l^{-1})	5	10	15	20	25
$k \times 10^{-5}$ (s^{-1})	10.2	17.8	9.4	8.8	3.3

Influence of TiO_2 particle size

The approach that we have found to be most useful for the investigation of surface area relationship with the particle size of the photocatalyst is representation of the kinetic data for contaminant degradation on a semi-log plot of particle size versus the corresponding rate constants. The results which are shown in Fig. 2 indicate that the rate constant of phenol red photocatalysis is steadily decreased with particle size increase. This could be elucidated by the possibility of the photoelectrons and photoholes generation in the bulk would, in smaller particles, have fewer traps and recombination centers to overcome before reaching the surface [44].

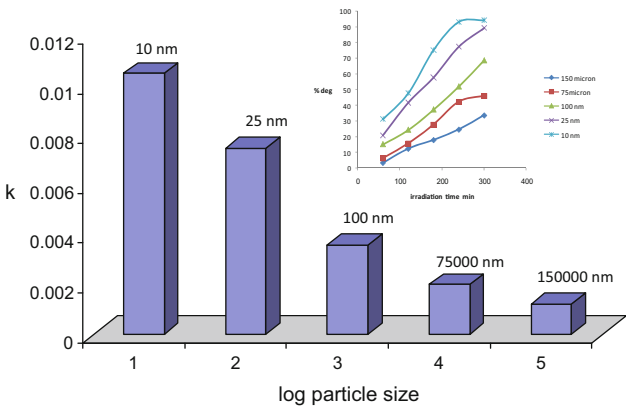

Fig. 2 Influence of TiO_2 particle size on the rate of photolysis. *Inset* shows degradation percent of phenol red at different particle sizes of TiO_2 particles

The particle sizes of TiO_2 seem to affect the photocatalytic degradation percent of phenol red under UV light irradiation as well, as it is clearly presented in Fig. 2, inset. This prediction has been verified as the degradation percent of the phenolic moiety is significantly promoted when the available active surface area for the photolysis process is higher.

Some researchers [34, 45, 46] have also observed similar impacts of particle size on kinetics and degradation yield in photooxidation processes. Shih and Lin [34] concluded that the effect of average particle size of TiO_2 nanoparticle aggregates for the degradation of azo dye has a special limit, while, Pichat et al. [46] reported that the rate of photodegradation of organic moieties is directly proportional with the surface area of TiO_2 nanoparticles and further, Khan et al. [45] concluded that the lower particle sizes of CeO_2 are responsible for their higher sensitivity and photocatalytic activity.

Impact of light intensity

Photocatalytic reaction rate depends largely on the radiation absorption of the photocatalyst [8], where the increase in light intensity enhances the degradation rate and yield in photocatalytic degradation. Vulliet et al. [24] have reported in their work on the photodegradation of cinosulfuron in aqueous TiO_2 suspension that there are two distinguished domains in this aspect: in the first one, at low light intensities (0–14 mW cm^{-2}), the rate would increase linearly with increasing light intensity (first-order), whereas at intermediate light intensities, above 14 mW cm^{-2}, the rate would depend on the square root of the light intensity (half order). This is likely, because at low light intensity, reactions involving electron–hole formation are predominant, and electron–hole recombination is negligible. However, at increased light intensity, electron–hole pair separation competes with recombination, thereby causing lower effect on the reaction rate.

Figure 3, which shows the result of the effect of UV light intensity on the initial degradation rate of phenol red in this study, is in a good accordance with the above approach. This enhancement of the rate of photodecolorization, as the light intensity increased, was also observed by other researchers [35, 40].

Malato et al. [31] have reported in their overview and trends for the solar photocatalysis of water that the typical Solar UV-flux of 20–30 Wm^{-2} is equivalent to 0.2–0.3 mol photons (Einstein) $m^{-2}\,h^{-1}$ in the 300–400 nm range. Accordingly, the intensity magnitudes which are employed in this work (shown in Table 4) correspond to 0.97, 2.23, and 10.8 mW cm^{-2}, and the rates, consequently, are increasing with increasing light intensity, which is stand-alone verification for the first-order process. These tentative findings are explicitly concerted with the published outcomes of other researchers [24, 29].

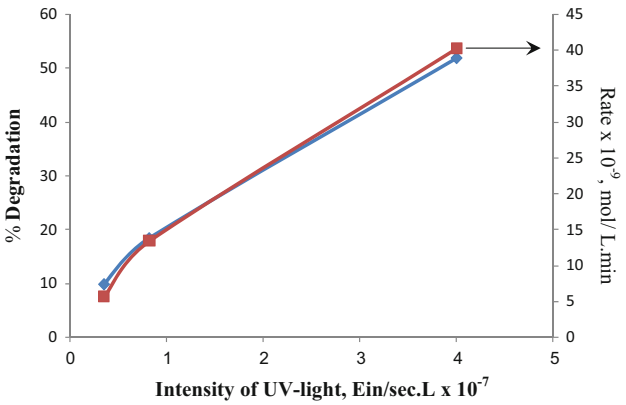

Fig. 3 Variations of the initial rate and degradation yield as a function of light source intensity

Table 4 Quantum yields of photodegradation of phenol red obtained at different intensities

Intensity (E l^{-1} s × 10^{-7})	Rate (mol l^{-1} s × 10^{-9})	Quantum yield Φ (%)
0.36	0.094	0.26
0.826	0.223	0.27
4	0.67	0.16

For further scrutinization and better evaluation of the efficiency of photocatalytic and photobleaching processes, we estimated the quantum yield Φ, which is defined as the ratio of the number of converted molecules per second to the number of efficient photons reaching the surface per second. The values of Φ are reported in Table 4. The maximum quantum yields are obtained for the lower light intensities, which are inline with the foregoing literature trend.

Effect of H_2O_2

The electron/hole (e^-/h^+) recombination is considered as one of the main problems in the application of TiO_2 photocatalysis. Accordingly, Malato and his colleagues [31] have reported that one of the most accepted strategies for inhibiting e^-/h^+ recombination has been the addition of other electron acceptors to the reaction.

Molecular oxygen is generally used as an electron acceptor in heterogeneous photocatalytic reaction [7]. However, Fig. 4 exhibits only about 60 % photobleaching of phenol red in the presence of O_2 gas solely, at the absence of H_2O_2, whereas the photodegradation yield has been found to be enhanced dramatically (>91 %) using hydrogen peroxide as an alternative electron acceptor. This is in accordance with the findings of Oghenejoboh et al. [27] who stated that the photocatalytic degradation of water effluent pollutants could be enhanced by addition of H_2O_2, because it is a better electron acceptor than oxygen.

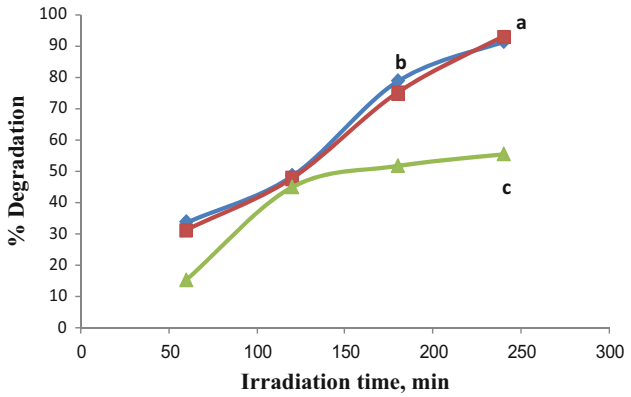

Fig. 4 Photodegradation of phenol red at **a** presence of both O_2 and H_2O_2. **b** Presence of only H_2O_2. **c** Presence of only O_2

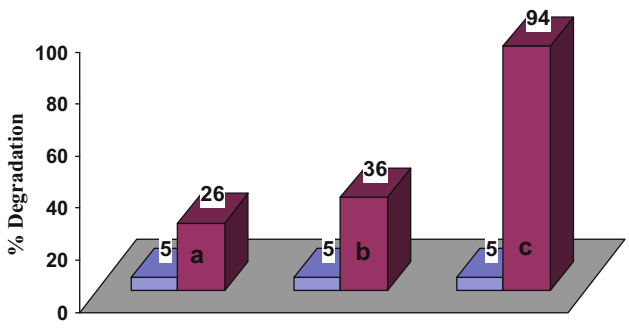

Fig. 5 Degradation yields of phenol red after 5 h UV photolysis under optimum experimental conditions for; **a** $TiO_2 + H_2O_2 + O_2$ gas (without irradiation); **b** $H_2O_2 + O_2$ gas + irradiation (without TiO_2); **c** $TiO_2 + H_2O_2 + O_2$ gas + irradiation; pH = 4.5, C_o = 10 mg l^{-1}, H_2O_2 = 3 mmol, TiO_2 = 0.5 g l^{-1}

On the other hand, our experimental outcomes verified that better efficiency of photodegradation process could be achieved (>94 % degradation) by application of both oxygen gas and hydrogen peroxide in combination with TiO_2 (Fig. 4). The positive sign of H_2O_2 addition indicated that there was a direct relationship between the initial H_2O_2 concentration and the yield of phenol red dye degradation, which increased by increasing H_2O_2 concentration, i.e., the presence of H_2O_2 in the reaction mixture plays a key role in the photocatalytic process which is in agreement with several authors [25, 27, 47].

We believe it is necessary to discuss, in detail, some aspects related to the effect of this electron acceptor. The addition of H_2O_2 has been found to be beneficial, increasing the degradation yield, due to its electron acceptor nature. This beneficial effect can easily be explained in terms of (a) additional production of $^{\cdot}OH$, which is a very strong oxidizing agent with standard redox potential of +2.8 V [29] through the following reactions under UV light radiation [29, 31]:

$$H_2O_2 + e^-_{CB} \rightarrow {}^{\cdot}OH + {}^{-}OH \quad (3)$$

$$H_2O_2 + h\nu \rightarrow {}^{\cdot}OH + {}^{\cdot}OH \quad (4)$$

$$H_2O_2 + O_2^{\cdot-} \rightarrow {}^{\cdot}OH + {}^{-}OH + O_2. \quad (5)$$

In addition, (b) inhibition of e^-/h^+ recombination could be explained in terms of TiO_2 surface modification by H_2O_2 adsorption and scavenging of photoproduced holes following the upcoming reaction:

$$H_2O_2 + 2h^+_{vb} \rightarrow O_2 + 2H^+. \quad (6)$$

Hence, the described reactions above indicate that hydroxyl radicals are more likely to form in UV/TiO_2/H_2O_2 systems, and other oxidizing species can also appear in the e^-/h^+ generation process.

Figure 5 depicts a relatively low degradation yield for phenol red/H_2O_2/O_2 system is achieved when only TiO_2 is used in dark (26 %) or when TiO_2 is absent (36 %). However, phenol red could be degraded appreciably (94 %) in this system by UV source illuminated TiO_2. Accordingly, these experiments demonstrated that H_2O_2, O_2 gas, UV irradiation, and the TiO_2 photocatalyst are needed for the effective photolysis of phenol red dye.

For further analysis of UV/TiO_2/H_2O_2 system which has been employed in this study, the plots of ln A_t (as first-order index) and $1/A_t$ (as second order index) versus time were established to devote the R^2 values as one of the methodologies to assign the pseudo order of the photocatalytic degradation process of phenol red dye in the presence of hydrogen peroxide. This mathematical technique has also been adopted by other researchers [11, 48]. Figure 6 presents R^2 values of 0.944 and 0.910 for ln A_t versus time, as pseudo-first-order evidence for the phenol red photodegradation process, using the UV/TiO_2/H_2O_2 and UV/TiO_2/O_2/H_2O_2 systems, respectively. Whereas, the poor R^2 values of 0.764 and 0.681 for $1/A_t$ versus time, as pseudo-second-order indicator for the phenol red photodegradation process, reveal explicitly that the UV/TiO_2/H_2O_2 and UV/TiO_2/O_2/H_2O_2 systems do not follow pseudo-second-order mechanism, since they did not exhibit a linear behavior during photolysis reaction of phenol red. This finding agrees well with Garcia et al. [11] who concluded that the degradation of the real textile organic effluents happens through pseudo-first-order reaction when UV/TiO_2/H_2O_2 system is employed.

Langmuir–Hinshelwood kinetic model

In recent years, the Langmuir–Hinshelwood (L–H) rate expression has been used successfully for heterogeneous

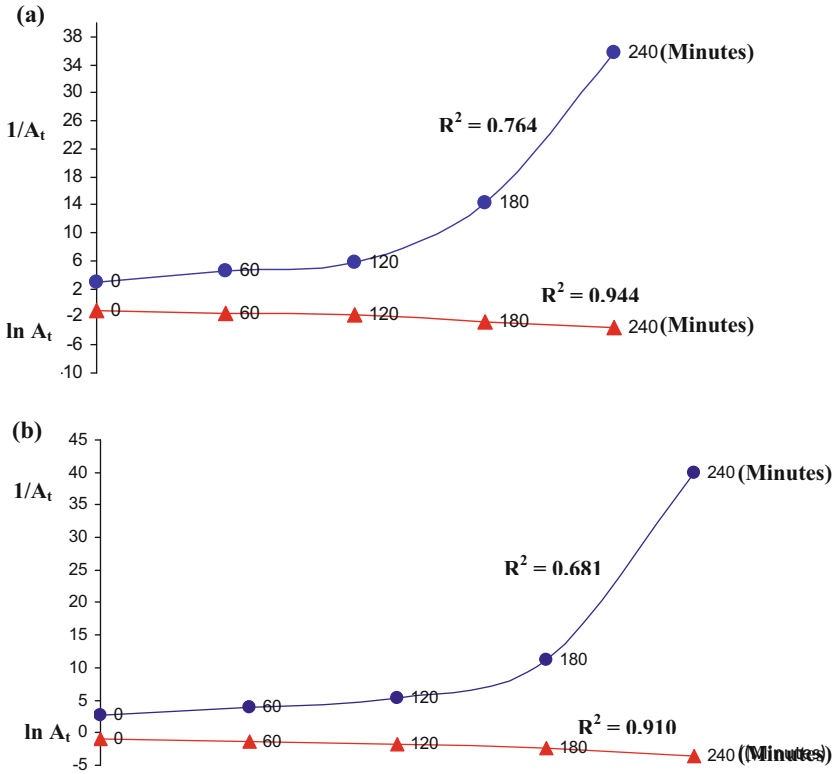

Fig. 6 Pseudo order of phenol red degradation with O_2 gas and H_2O_2 (A_t absorbance at time t and 432 nm: **a** only H_2O_2; and **b** O_2 gas and H_2O_2

photocatalytic degradation to elucidate the relationship between initial degradation rate and initial concentration [36]. Furthermore, the Langmuir–Hinshelwood model is usually used to describe the kinetics of photocatalytic process [30]. The derivation is based on the degradation rate (r), which is expressed as follows:

$$r = -\mathrm{d}C_0/\mathrm{d}t = (k_r K_{ad} C_0)/(1 + K_{ad} C_0) \quad (7)$$

where r represents the initial rate of photooxidation (mol or mg l^{-1} min), C_0 the concentration of the reactant (mol or mg l^{-1}), t the irradiation time, k_r the rate constant of the reaction (mol or mg l^{-1} min), and K_{ad} is the adsorption equilibrium coefficient of the reactant (l mg^{-1} or mol). Assuming that adsorption is weak and the concentration of the organic moiety is low, Eq. (7) can be simplified to the first-order kinetics expression with an apparent rate constant (k_{app}) [29]:

$$\ln(C_0/C_t) = kK_t = K_{app} t \quad (8)$$

or

$$C_t = C_0 e^{-k_{app} t}. \quad (9)$$

From the perspective of linear algebra, the plot of ln (C_t/C_0) as a function of reaction time, t, should have linear relationship and its slope is the apparent rate constant.

Hence, the plot of $\ln(C_t/C_0)$ versus reaction time t with different initial phenol red concentrations, C_0, is shown in Fig. 7. It was found that the linear relationship was good

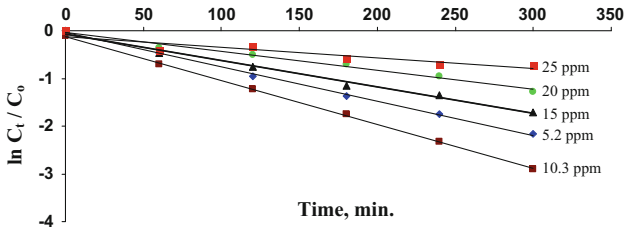

Fig. 7 Plot of $\ln(C_t/C_0)$ versus reaction time at different initial concentrations of phenol red (catalyst loading = 0.5 g l^{-1}; pH = 4.5)

and rate constant k_{app} declined generally with increasing initial concentrations of phenol red beyond optimum concentration.

Equation (7) could be modified to linear-type equation as presented in the following:

$$1/r = 1/k_r + 1/k_r K_{ad} C_0 \quad (10)$$

Plot of reciprocal reaction rate $1/r$ versus reciprocal initial concentration $1/C_0$ (from Eq. 12) is presented in Fig. 8. A reasonable fit of this equation was obtained with values of 0.0045 μM^{-1} (0.0127 ppm^{-1}) and 0.0333 $\mu M\ s^{-1}$ for K_{ad} and k_r, respectively. This indicates that the degradation of phenol red occurred mainly on the surface of TiO_2. However, Turchi and Ollis [49] investigated the photodegradation of organic pollutants in illuminated TiO_2 slurries and found it plausible that the reaction occurs not only on the TiO_2 surface, but also in solution.

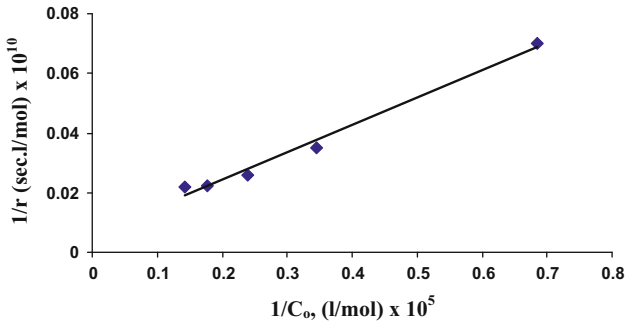

Fig. 8 Langmuir–Hinshelwood model outcomes for the disappearance of phenol red at different initial concentrations; TiO_2 loading = 0.5 g l^{-1}; pH = 4.5

The foregoing value of K_{ad} refers to the strong adsorption of phenol red moiety onto the electrophilic (Ti^{4+}) sites at the TiO_2 surface. Some authors [13, 50] reported that the adsorption linkages of phenol red onto TiO_2 surface bridged through sulphonato and phenolic anchoring groups.

UV–VIS–FTIR spectral study

UV–VIS absorption profile

To examine the response of photocatalytic activities of nanoTiO_2, the absorption spectra of exposed samples at various time intervals were recorded, and the rate of decolorization was observed in terms of change in the main intensity at λ_{max} (432 nm) of the dye.

Figure 9 presents typical UV–VIS spectra of three absorption bands for phenol red (10 mg l^{-1}) located at 263, 432, and 590 nm. The main two visible region bands which are located at 432 and 590 nm, attributed to the chromophoric structure, whereas the band located at 263 nm is assigned to benzoic ring [26, 51]. The counter-intuitive appearance of the band located at 590 nm in acidic medium (pH = 4.5) supports the high stability of the keto form, which is usual in basic medium as a keto-enol tautomerism product, due to the conjugation of the molecule.

The percentage of decolorization efficiency of samples has been calculated for the most intense absorption peak at 432 nm as follows [52]:

$$\text{Efficiency } \% = 100\{(A_0 - A_t)/A_0\} \quad (11)$$

where A_0 and A_t are initial absorbance and absorbance after irradiation at various time intervals, respectively. Also, from Fig. 9 (inset), which represents the time-dependent UV–Vis absorption spectra of phenol red during irradiation with nanoTiO_2 under UV light, it was found that TiO_2 decolorizes phenol red evidently after 300 min of irradiation.

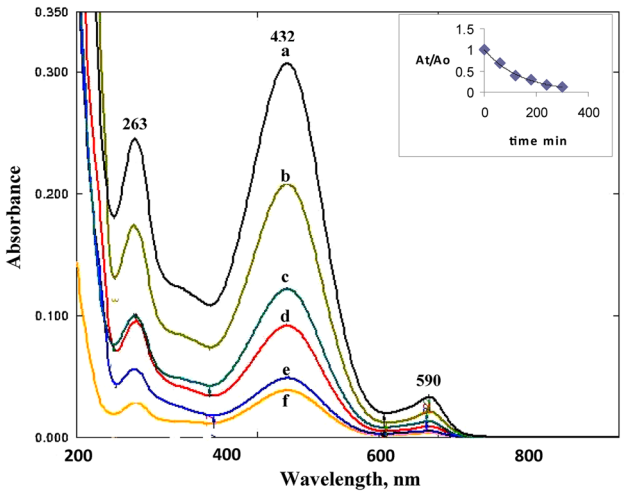

Fig. 9 UV–VIS spectra changes of phenol red (10 mg l^{-1}) in aqueous nanoTiO_2 dispersion (0.5 g l^{-1}) irradiated under UV light at varying times: *a* 0, *b* 1, *c* 2, *d* 3, *e* 4, and *f* 5 h. *Inset* shows the normalized absorbance at 432 nm

Under optimum operational conditions namely, pH = 4.5, nanopowder loading = 0.5 g l^{-1}, UV light intensity = 485 × 10^{-10} Ein s^{-1} L and pollutant concentration = 10.3 ppm, we have observed a gradual photodecolorization of the polluted solution over 5 h of irradiation vanishing >90 % of the pollutant. Also, from Fig. 9, increasing in the illumination time allows the absorption spectra to be shifted exponentially and vertically toward the low absorbance values for the main absorption band, 432 nm, suggesting that the chromophore responsible for the characteristic color of the compound is destructed and subsequently degraded down. Furthermore, no new absorption bands appeared in either the visible or the UV spectra regions. This is also accompanied by simultaneous decrease of the intensities of other bands, 263 and 590 nm.

FTIR characterization of phenol red-TiO_2 system

For the description of the interaction between phenol red dye and TiO_2 catalyst, the Fourier transform infrared (FTIR) technique has been exploited. Figure 10 shows the FTIR spectra of phenol red and phenol red bound to TiO_2. The spectrum of pure phenol red showed the sulphonato group stretching at 1462 cm^{-1}. Similar band (1480 cm^{-1}) has also been assigned by Asiri et al. [13]. This band is completely disappeared in the spectrum of phenol red bound TiO_2. Furthermore, the sharp stretching band at 3398 cm^{-1} is attributed to the OH group in the pure phenol red [53]. This band disappeared, as well, and a new broad band appeared at 3275 cm^{-1}. This confirms the adsorption of phenol red

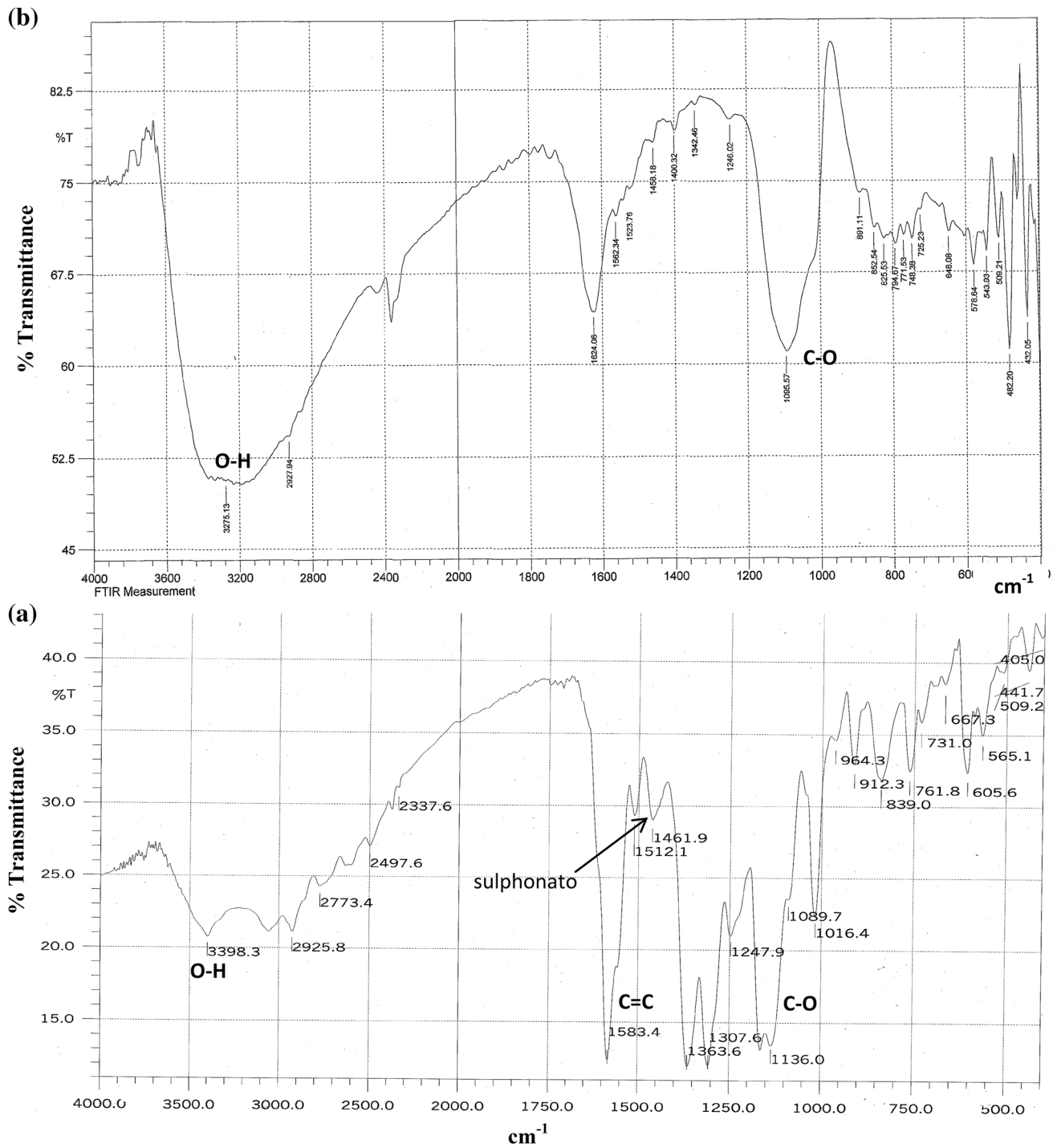

Fig. 10 FTIR spectra of pure phenol red (**a**) and phenol red adsorbed onto TiO_2 (**b**)

on TiO_2 surface as other anchoring groups [54]. Moreover, the appearance of a band at $\sim$1096 cm^{-1} for phenol red/TiO_2 spectrum is verification for the adsorption of phenol red onto TiO_2 and subsequent degradation. On the other hand, the shifts in the stretching frequencies of OH and C–O groups that have also been reported previously by some computational authors [50, 55] are ascribed to the adsorption onto TiO_2 powder particles.

On the basis of above findings, we report here that the interaction of phenol red with TiO_2 surface occurs through its sulphonato- and phenolic-collaging groups.

Thermodynamic functions

The effect of temperature on photodegradation process of phenol red dye in aqueous TiO_2 suspension was studied at various temperatures in the range from 293 to 318 K. The apparent rate constant (k_{app}) was evaluated at each temperature. An increase of degradation was observed with increasing temperature. The apparent rate constant and temperature can be expressed by Arrhenius relation as follows [23]:

$$k_{app} = Ae^{-E_a/RT} \quad (12)$$

where k_{app} is the apparent rate constant, A is the frequency factor or pre-exponential factor, E_a is the activation energy of the reaction, R is general gas constant (8.314 J mol^{-1} K^{-1}), and T is the absolute temperature.

Translation of Eq. (12) resulted in the following equation;

$$\ln k_{app} = \ln A - E_a/RT. \quad (13)$$

A linear plot of ln k_{app} versus $1/T$ yielded a straight line (Fig. 11) from which the activation energy can be obtained and is given in Table 5. Chen and Ray [36] reported that the increase in rate constant is most likely due to the increasing collision frequency of molecules in the solution that increases with increasing temperature.

The other thermodynamic parameters for instance free energy of activation ($\Delta G^{\#}$), enthalpy of activation($\Delta H^{\#}$), and entropy of activation ($\Delta S^{\#}$) were calculated (Table 5) using activation energy and apparent rate constant, and employing Eyring's equation as follows [56, 57]:

$$k_{app} = k_B T/h \text{ exponential } \left(-\Delta G^{\#}/RT\right). \quad (14)$$

Equation (13) can be rewritten as [58]:

$$d\left(\ln k_{app}\right)/dT = E_a/RT^2. \quad (15)$$

Likewise, Eq. (14) is rewritten as:

$$\ln k_{app} = \ln(k_B T/h) - \Delta H^{\#}/RT + \Delta S^{\#}/R, \quad (16)$$

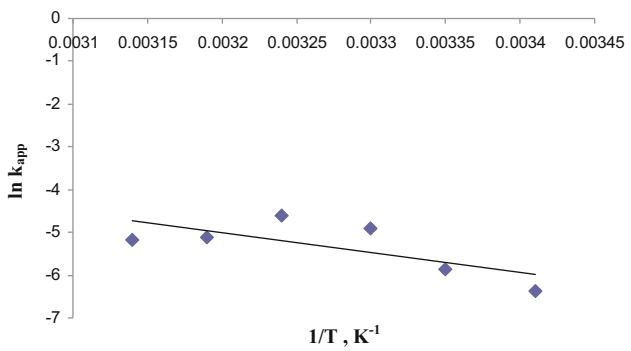

Fig. 11 Variation in apparent reaction rate with operational temperature (pH = 4.5; catalyst dosage = 0.5 g l^{-1}; C_0 = 10 mg l^{-1})

Solving Eqs. (15) and (16) for the activation enthalpy gives

$$\Delta H^{\#} = E_a - RT. \quad (17)$$

Finally, giving access to the entropy of activation

$$\Delta S^{\#} = \left(\Delta H^{\#} - \Delta G^{\#}\right)/T \quad (18)$$

where k_B is Boltzmann constant (1.3805 × 10^{-23} J K^{-1}), and h is Planck's constant (6.6256 × 10^{-34} J s).

From Table 5, it can be concluded that TiO_2-mediated photocatalytic degradation of phenol red is slightly affected by temperature change. Similar conclusion was drawn by other researchers [44, 59]. Nevertheless, an increase in temperature facilitates the reaction to compete more efficiently with electron–hole pair recombination. Also, from Fig. 11, we observed a decrease in the degradation rates at temperatures of 313 and 318 K. This could be most likely ascribed to desorption of phenol red dye at these temperatures, as long as the adsorption–desorption equilibrium plays a key role in the photocatalytic process, which is already verified through the estimated adsorption coefficient of phenol red in this work. Several authors reported experimental evidence for the dependence of photocatalytic activity on temperature [59, 60]. Furthermore, Soares et al. [60] stated that at a relatively high temperature (40–60 °C), the limiting stage becomes the adsorption of the dye on the TiO_2. Nevertheless, Gogate and Pandit [32] concluded that a photocatalytic reaction has a point or an optimum range of operation between 20 and 80 °C. Whereas, Ibrahim and Abdullah [8] reported that the increase in temperature enhances the recombination of charge carriers and desorption process of adsorbed reactant species, resulting in decrease of photocatalytic activity. Based on the above argument, it can be concluded that the temperature dependent steps in photocatalytic reaction are adsorption and desorption of reactants and products on the surface of photocatalyst.

Reusability of the synthesized nanoanatase TiO_2

To examine the stability and reusability efficiency of the prepared nanoanatase TiO_2 particles, the reusability of the photocatalyst was explored. The recovered TiO_2 nanopowder was reused for four consecutive runs without calcination, whereas the fifth run was carried out after calcination of the recovered TiO_2 nanopowder at 400 °C for 4 h. Table 6 demonstrates a steady decrease in the activity of TiO_2 photocatalyst over four consecutive uses and an increase in the activity during the fifth run upon calcination. This strongly indicates on one hand, that the nature of the catalyst did not change during photocatalysis, and on the other hand, there is a quantitative adsorption of the phenol red on the surface of the catalyst.

Table 5 Thermodynamic parameters for the photocatalytic degradation of phenol red

T (K)	E_a (kJ mol^{-1})	$\Delta G^{\#}$ (kJ mol^{-1})	$\Delta H^{\#}$ (kJ mol^{-1})	$\Delta S^{\#}$ (JK^{-1} mol^{-1})
293	38.227	87.25	35.79	−176
298		87.55	35.75	−174
303		86.57	35.71	−168
308		87.31	35.66	−168
313		90.10	35.62	−174
318		91.76	35.58	−177

Table 6 Impact of nanoTiO_2 reuse on photodegradation of phenol red

Number of runs	1	2	3	4	5[a]
Normalized deg. (%)	100	76	53	32	66

[a] Run 5 refers to calcined TiO_2 at 400 °C after four irradiation cycles

Conclusions

The influences of several operational parameters, namely, phenol red initial concentration, TiO_2 dosage, particle size, UV light intensity, and varying of photolysis solution pH, have been evaluated: the photocatalytic reaction is favored by a low particle size nanocatalyst and relatively a high light intensity, whereas the best efficiency is obtained for 0.5 g l^{-1} TiO_2 dosage, photolysis solution pH of 4.5, and 10.3 ppm of initial dye concentration.

The kinetics of the photocatalytic oxidation follows a Langmuir–Hinshelwood model which demonstrates the pseudo-first-order with respect to the dye initial concentration within the experimental concentration range. The rate of the photocatalytic degradation was enhanced by the addition of H_2O_2. Hydroxyl radicals contributed appreciably, other than O_2 gas, in the photobleaching process indicating the remarkable role of hydroxyl type chemistry mechanism in the process. On the other hand, an increase of the temperature has kind effect on kinetics and facilitates the degradation process to good extent. The effect of temperature from 293 to 318 K showed that the apparent rate constants follow the Arrhenius relation. The activation energy of the degradation of phenol red was found to be 38 kJ mol^{-1}.

Acknowledgments The authors wish to thank Georgia Institute of Technology/Atlanta/Georgia/USA for providing of the analytical instruments.

References

1. Wahab, H.S.: Molecular modeling of the adsorption and initial photocatalytic oxidation step for *para*-nitrophenol on nano-sized TiO_2 surface. Surf. Sci. **606**, 624–633 (2012)
2. Koyuncu, H., Yildiz, N., Salgin, U., Koroglu, F., Calimli, A.: Adsorption of *o*-, *m*- and *p*-nitrophenols onto organically modified bentonites. J. Hazard. Mater. **185**, 1332–1339 (2011)
3. Wahab, H.S., Koutselos, A.D.: Computational modeling of the adsorption and ˙OH initiated photochemical and photocatalytic primary oxidation of nitrobenzene. J. Mol. Model. **15**, 1237–1244 (2009)
4. Ahmed, S., Rasul, M.G., Brown, R., Hashib, M.A.: Influence of parameters on the heterogeneous photocatalytic degradation of pesticides and phenolic contaminants in waste water: a short review. J. Environ. Manag. **92**, 311–330 (2011)
5. Dixit, A., Tirpude, A.J., Mungray, A.K., Chakraborty, M.: Degradation of 2,4 DCP by sequential biological-advanced oxidation process using UASB and UV/TiO_2/H_2O_2. Desalination **272**, 265–269 (2011)
6. González, L.F., Sarria, V., Sánchez, O.F.: Degradation of chlorophenols by sequential biological-advanced oxidative process using *Trametes pubescens* and TiO_2/UV. Bioresour. Technol. **101**, 3493–3499 (2010)
7. Teh, C.M., Mohamed, A.: Roles of titanium dioxide and ion-doped titanium dioxide on photocatalytic degradation of organic pollutants (phenolic compounds and dyes) in aqueous solutions: a review. J. Alloy. Compd. **509**, 1648–1660 (2011)
8. Ibrahim, G.U., Abdullah, A.H.: Heterogeneous photocatalytic degradation of organic contaminants over titanium dioxide: a review of fundamentals, progress and problems. J. Photochem. Photobiol. C Photochem. Rev. **9**, 1–12 (2008)
9. Song, S., Hong, F., He, Z., Cai, Q., Chen, J.: $AgIO_3$-modified AgI/TiO_2 composites for photocatalytic degradation of *p*-chlorophenol under visible light irradiation. J. Colloid. Interface. Sci. **378**, 159–166 (2012)
10. Wahab, H.S., Koutselos, A.D.: A computational study on the adsorption and OH initiated photochemical and photocatalytic primary oxidation of aniline. Chem. Phys. **358**, 171–176 (2009)
11. Garcia, J.C., Oliveira, J.L., Silva, A.E.C., Oliveira, C.C., Nozaki, J., Souza, N.E.: Comparative study of the degradation of real textile effluents by photocatalytic reactions involving UV/TiO_2/H_2O_2, and UV/Fe^{2+}/H_2O_2 systems. J. Hazard. Mater. **147**, 105–110 (2007)
12. Schiavello, M. (ed.): Heterogeneous Photocatalysis. Wiley Series in Photoscience and Photoengineering, vol. 3. Wiley, Oxford (1997)
13. Asiri, A.M., Al-Amoudi, M.S., Al-Talhi, T.A., Al-Talhi, A.D.: Photodegradation of Rhodamine 6G and phenol red by nanosized TiO_2 under solar irradiation. J. Saudi Chem. Soc. **15**, 121–128 (2011)
14. Tan, T.K., Khiew, P.S., Chiu, W.S., Radiman, S., Abd-Shukor, R., Huang, N.M., Lim, H.N.: Photodegradation of phenol red in

the presence of ZnO nanoparticles. Int. J. Chem. Molec. Nucl. Mater. Metall. Eng. **5**, 613–618 (2011)
15. Wong, S.T., Hwang, C.C., Mou, C.Y.: Tungstated zirconia catalyzed bromination of phenol red under nearly neutral solution. Appl. Catal. B. Environ. **63**, 1–8 (2006)
16. Zaggout, F.R.: Entrapment of phenol red pH indicator into a sol–gel matrix. Mater. Lett. **60**, 1026–1030 (2006)
17. Jiu, J., Isoda, S., Adachi, M., Wang, F.: Preparation of TiO_2 nanocrystalline with 3–5 nm and application for dye-sensitized solar cell. J. Photochem. Photobiol. A Chem. **189**, 314–321 (2007)
18. Chiu, W.S., Khiew, P.S., Cloke, M., Isa, D., Tan, T.K., Radiman, S., Abd-Shukor, R., Abd-Hamid, M.A., Huang, N.M., Lim, H.N., Chia, C.H.: Photocatalytic study of two-dimensional ZnO nanopellets in the decomposition of methylene blue. Chem. Eng. J. **158**, 345–352 (2010)
19. Tan, T.K., Khiew, P.S., Chiu, W.S., Radiman, S., Abd-Shukor, R., Huang, N.M., Lim, H.N.: Photodegradation of phenol red in the presence of ZnO nanoparticles. Int. J. Chem. Mol. Nucl. Mater. Metall. Eng. **5**, 613–618 (2011)
20. Wahab, H.S.: Quantum chemical modeling study of adsorption of benzoic acid on anatase TiO_2 nanoparticles. J. Mol. Model. **18**, 2709–2716 (2012)
21. Brus, L.E.: Electron–electron and electron hole interactions in small semiconductor crystallites: the size dependence of the lowest excited electronic state. J. Chem. Phys. **80**, 4403–4412 (1984)
22. Zhao, W., Wu, Z., Shi, H., Wang, D.: UV photodegradation of azo dye diacryl red X-GRL. J. Photochem. Photobiol. A Chem. **171**, 97–106 (2005)
23. Naeem, K., Weiqian, P., Ouyang, F.: Thermodynamic parameters of activation for photodegradation of phenolics. Chem. Eng. J. **156**, 505–509 (2010)
24. Vulliet, E., Emmelin, C., Chovelon, J.M., Guillard, C., Hermann, J.M.: Photocatalytic degradation of the herbicides cinosulfuron in aqueous TiO_2 suspension. Environ. Chem. Lett. **1**, 62–67 (2003)
25. Cherif, L.Y., Yahiaoui, I., Benissad, F.A., Madi, K., Benmehdi, N., Fourcade, F., Amrane, A.: Heat attachment method for the immobilization of TiO_2 on glass plates: application to photodegradation of basic yellow dye and optimization of operating parameters, using response surface methodology. Ind. Eng. Chem. Res. **53**, 3813–3819 (2014)
26. Tamura, Z., Maeda, M.: Differences between phthaleins and sulfonphthaleins (in Japanese). Yakugaku Zasshi **117**, 764–770 (1997). **(PMID 9414589)**
27. Oghenejoboh, K.M., Aisien, F.A., Ihoeghian, N.: Photocatalytic degradation of chlorobenzene in aqueous solutions-comparison of TiO2 with Periwinkle and Snail Shells' powder as photo catalyst. Br. J. Appl. Sci. Technol. **4**, 808–822 (2014)
28. Wang, K.H., Hsieh, Y.H., Chen, L.J.: The heterogeneous photocatalytic degradation, intermediates and mineralization for the aqueous solution of cresols and nitrophenols. J. Hazar. Mater. **59**, 251–260 (1998)
29. Konstantinou, I.K., Albanis, T.A.: TiO_2-assisted photocatalytic degradation of azo dyes in aqueous solution: kinetic and mechanistic investigations: a review. Appl. Catal. B Environ. **49**, 1–14 (2004)
30. Zhang, Y., Selvaraj, R., Sillanpä, M., Kim, Y., Tai, C.W.: The influence of operating parameters on heterogeneous photocatalytic mineralization of phenol over $BiPO_4$. Chem. Eng. J. **245**, 117–123 (2014)
31. Malato, S., Fernandez-Ibanez, P., Maldonado, M.I., Blanco, J., Gernjak, W.: Decontamination and disinfection of water by solar photocatalysis: recent overview and trends. Catal. Today **147**, 1–59 (2009)
32. Gogate, P.R., Pandit, A.B.: A review of imperative technologies for wastewater treatment I: oxidation technologies at ambient conditions. Adv. Environ. Res. **8**, 501–551 (2004)
33. Hermann, J.M.: Heterogeneous photocatalysis: fundamentals and applications to the removal of various types of aqueous pollutants. Catal. Today **53**, 115–129 (1999)
34. Shih, Y., Lin, C.: Effect of particle size of titanium dioxide nanoparticle aggregates on the degradation of one azo dye. Environ. Sci. Pollut. Res. **19**, 1652–1658 (2012)
35. Sakthivel, S., Neppolian, B., Shankar, M.V., Arabindoo, B., Palanichamy, M., Murugesan, V.: Solar photocatalytic degradation of azo dye: comparison of photocatalytic efficiency of ZnO and TiO_2. Solar Energy Mater. Solar Cells **77**, 65–82 (2003)
36. Chen, D., Ray, A.K.: Photodegradation kinetics of 4-nitrophenol in TiO_2 suspension. Water Res. **32**, 3223–3234 (1998)
37. Behnajady, M.A., Modirshahla, N., Shokri, M., Elham, H., Zeininezhad, A.: The effect of particle size and crystal structure of titanium dioxide nanoparticles on the photocatalytic properties. J. Environ. Sci. Health A **43**, 460–467 (2008)
38. Andronic, L., Enesca, A., Vladuta, C., Duta, A.: Photocatalytic activity of cadmium doped TiO_2 films for photocatalytic degradation of dyes. Chem. Eng. J. **152**, 64–71 (2009)
39. Daneshvar, N., Salari, D., Khataee, A.R.: Photocatalytic degradation of azo dye acid red 14 in water: investigation of the effect of operational parameters. J. Photochem. Photobiol. A Chem. **157**, 111–116 (2003)
40. Neppolian, B., Choi, H.C., Sakthivel, S., Arabindoo, B., Murugesan, V.: Solar light induced and TiO_2 assisted degradation of textile dye reactive blue 4. Chemosphere **46**, 1173–1181 (2002)
41. Chio, C.H., Wu, C.Y., Juang, R.S.: Photocatalytic degradation of phenol and *M*-nitrophenol using irradiated TiO_2 in aqueous solutions. Sep. Purif. Technol. **62**, 559–564 (2008)
42. Selvam, K., Muruganandham, M., Muthuvel, I., Swaminathan, M.: The influence of inorganic oxidants and metal ions on semiconductor sensitized photodegradation of 4-flurophenol. Chem. Eng. J. **128**, 51–57 (2007)
43. Su, Y., Deng, L., Zhang, N., Wang, X., Zhu, X.: Photocatalytic degradation of C.I. acid blue 80 in aqueous suspensions of titanium dioxide under sunlight. React. Kinet. Catal. Lett. **98**, 228–230 (2008)
44. Hussein, F.H.: Photochemical treatments of textile industries wastewater. In: Hauser, P. (ed.) Advances in Treating Textile Effluent. Intech Publishing Company, Croatia (2011)
45. Khan, S.B., Faisal, M., Rahman, M.M., Akhtar, K., Asiri, A.M., Khan, A., Alamry, K.A.: Effect of particle size on the photocatalytic activity and sensing properties of CeO_2 nanoparticles. Int. J. Electrochem. Sci. **8**, 7284–7297 (2013)
46. Pichat, P., Guillard, G., Maillard, C., Amatric, L., Doliveira, J.C.: In: Ollis, D.F., El-Ekabi, H. (eds.) Photocatalytic Purification of Water and Air. Elsevier, Amsterdam (1993)
47. Lodha, S., Vaya, D., Ameta, R., Punjabi, P.B.: Photocatalytic degradation of phenol red using complexes of some transition metals and hydrogen peroxide. J. Serb. Chem. Soc. **73**, 631–639 (2008)
48. Fayoumi, L.M.A., Ezzedine, M.A., Akel, H.H., El Jamal, M.M.: Kinetic study of the degradation of crystal violet by $K_2S_2O_8$. Comparison with Malachite Green. Port. Electrochim. Acta **30**, 121–133 (2012)
49. Turchi, C.S., Ollis, D.F.: Photocatalytic degradation of organic water contaminants: mechanisms involving hydroxyl radical attack. J. Catal. **122**, 178–192 (1990)
50. Wahab, H.S., Bredow, T., Aliwi, S.M.: A computational study on the adsorption and ring cleavage of *para*-chlorophenol on anatase TiO_2 surface. Surf. Sci. **603**, 664–669 (2009)

51. Movahedi, M., Mahjoub, A.R., Janitabar-Darzi, S.: Photodegradation of Congo Red in aqueous solution on ZnO as an alternative catalyst to TiO_2. J. Iran. Chem. Soc. **6**, 570–577 (2009)
52. Chauhan, R., Kumar, A., Chaudhary, R.P.: Structural and photocatalytic studies of Mn doped TiO2 nanoparticles. Spectrochim. Acta Part A Mol. Biomol. Spect. **98**, 256–264 (2012)
53. http://www.chem.ucla.edu/~webspectra/irtable.html
54. Kathiravan, A., Renganathan, R.: Effect of anchoring group on the photosensitization of colloidal TiO_2 nanoparticles with porphyrins. J. Colloid Interface Sci. **331**, 401–407 (2009)
55. Wahab, H.S., Bredow, T., Aliwi, S.M.: Computational modeling of the adsorption and photodegradation of 4-chlorophenol on anatase TiO_2 particles. J. Mol. Struct. THEOCHEM **863**, 84–90 (2008)
56. Laidler, K., Meisler, J., Sanctuary, B.: Physical Chemistry, 4th edn. Houghton Mifflin, New York (2003)
57. Garsoux, G., Lamotte, J., Geraday, C., Feller, G.: Kinetic and structural optimization to catalysis at low temperatures in a psychrophilic cellulase from the Antarctic bacterium *Pseudoalteromonas haloplanktis*. Biochem. J. **384**, 247–253 (2004)
58. Lonhienne, T., Gerday, C., Feller, G.: Psychrophilic enzymes, revisiting the thermodynamic parameters of activation may explain local flexibility. Biochim. Biophys. Acta **1543**, 1–10 (2000)
59. Fu, X., Clark, L.A., Zeltner, W.A., Anderson, M.A.: Effects of reaction temperature and water vapor content on the heterogeneous photocatalytic oxidation of ethylene. J. Photochem. Photobiol. A Chem. **97**, 181–186 (1996)
60. Soares, E.T., Lansarin, M.A., Moro, C.C.: A study of process variables for the photocatalytic degradation of Rhodamine B. Braz. J. Chem. Eng. **24**, 29–36 (2007)